THESIS FOR THE DEGREE OF DOCTOR OF PHILOSOPHY

Computational modeling of trans- and intergranular fracture in polycrystals

Kim Louisa Auth

Department of Industrial and Materials Science
Chalmers University of Technology
Gothenburg, Sweden, 2024

Computational modeling of trans- and intergranular fracture in polycrystals

Kim Louisa Auth
ISBN 978-91-8103-121-8

Doktorsavhandlingar vid Chalmers tekniska högskola
Ny serie nr 5579
ISSN 0346-718X

Department of Industrial and Materials Science
Chalmers University of Technology
SE-412 96 Gothenburg, Sweden
Phone: +46 (0)31 772 1000

Cover:
The cover image shows a polycrystalline grain structure with a crack that extends by intergranular crack growth from the left via mixed inter- and transgranular crack growth in the middle to transgranular crack growth on the right. Embedded in the grain structure are visualizations of a chemo-mechanically coupled intergranular fracture simulation (left) and a transgranular fracture simulation with damage-dependent micro-flexible boundary conditions (right).

Printed by Chalmers Reproservice
Gothenburg, Sweden, November 2024

In Gedenken an Anita und Wolfgang.

Computational modeling of trans- and intergranular fracture in polycrystals

Kim Louisa Auth
Department of Industrial and Materials Science
Chalmers University of Technology

Abstract

Nickel-based superalloys are commonly used in demanding environments, where high temperatures are combined with considerable mechanical loads, such as turbine disks in jet engines and gas turbines. When exposed to a combination of severe loading conditions, including an oxygen-rich environment, high temperatures, and sustained tensile loading, the fracture mode of nickel-based superalloys can change from the default ductile transgranular fracture to environmentally assisted intergranular fracture.

In this thesis, a fully chemo-mechanically coupled modeling framework is presented for intergranular fracture. The framework is built on a cohesive zone law, that is degraded based on the local oxygen concentration. Oxygen transport is at the same time accelerated by traction gradients. The model is complemented by a moving oxygen boundary condition, which follows the crack tip upon crack propagation. It is demonstrated that the framework can qualitatively predict experimental results such as the reduction of ultimate tensile strength and the dependence of the average crack growth rates on the environmental oxygen content, load level, and dwell time in cyclic loading.

In order to capture the formation of transgranular cracks, a thermodynamical framework for ductile phase-field fracture is developed. It is based on a large deformation crystal plasticity model and incorporates size dependence via gradient-extended hardening. A micromorphic damage irreversibility approach is adopted to ensure thermodynamic and variational consistency of the proposed model. A damage dependent micro-flexible boundary condition for gradient-extended hardening is developed, which allows grain boundaries to retain their resistance to slip transmission during hardening. Numerical simulations show that the fracture model can describe transgranular crack growth in two- and three-dimensional polycrystals, while considering microstructural effects such as crystal orientation, grain geometry and void coalescence.

Keywords: Environmentally assisted fatigue, Intergranular fracture, Moving boundary condition, Transgranular fracture, Phase-field modeling, Gradient crystal plasticity, Micro-flexible boundary condition, Nickel-based superalloy.

List of Publications

This thesis is based on the following publications:

[A] **Kim Louisa Auth**, Jim Brouzoulis, Magnus Ekh, "A fully coupled chemo-mechanical cohesive zone model for oxygen embrittlement of nickel-based superalloys". *Journal of the Mechanics and Physics of Solids*, vol. 164, 140880, Jul. 2022. DOI: 10.1016/j.jmps.2022.104880.

[B] **Kim Louisa Auth**, Jim Brouzoulis, Magnus Ekh, "Modeling of environmentally assisted intergranular crack propagation in polycrystals ". *International Journal of Numerical Methods in Engineering*, vol. 124, issue 23, Dec. 2023. DOI: 10.1002/nme.7346.

[C] **Kim Louisa Auth**, Jim Brouzoulis, Magnus Ekh, "A thermodynamic framework for ductile phase-field fracture and gradient-enhanced crystal plasticity". *European Journal of Mechanics - A/Solids*, vol. 108, 105418, Nov.-Dec. 2024. DOI: 10.1016/j.euromechsol.2024.105418.

[D] **Kim Louisa Auth**, Jim Brouzoulis, Magnus Ekh, "Phase-field modeling of ductile fracture across grain boundaries in polycrystals". *Submitted for international publication*, Preprint available on arXiv. DOI: 10.48550/arXiv.2410.24107 .

The attached papers were prepared in collaboration with the co-authors. The author of this thesis was responsible for the majority of the work in all four articles, including planning and writing the papers, contributing to the development of the theory, developing the computational framework and implementing the numerical models, running the simulations, interpreting the results and managing the submission and peer review process.

Preface

This thesis is a result of my work at the Division of Material and Computational Mechanics, Department of Industrial and Materials Science, Chalmers University of Technology between January 2020 and November 2024. The project has been funded by the Swedish Research Council (Vetenskapsrådet) under the grant numbers 2018-04318 and 2018-06482. Part of the simulations were performed on resources at the Chalmers Centre for Computational Science and Engineering (C3SE) provided by the Swedish National Infrastructure for Computing (SNIC).

Acknowledgments

First and foremost, I would like to thank my supervisors Magnus Ekh and Jim Brouzoulis for their guidance, encouragement, and support. Thank you for always showing trust and appreciation for my work and for your patience with me. I feel very privileged for all the time you took to teach me, discuss with me, guide me in my professional decisions and for caring about both my personal development and my academic progress.

I want to thank the other `Ferrite.jl` devs, in particular Fredrik, Elias and Maximilian, collaborating with you has been so much fun! A special thank you goes to Fredrik Ekre, who introduced me to `Julia` and guided me through my first steps in open-source software development. I appreciate our discussions and am grateful for all of the computing knowledge you have shared with me. I am also happy and proud to be a part of Julia Gender Inclusive. The encouragement for each other and the can-do attitude in our community mean a lot to me.

My colleagues make coming to the office a joy. The warm, welcoming, and friendly environment here has made me want to stay from the beginning. All the coffees, kitchen and office chats, shared joy and frustration have made this a great journey. I also want to thank Alexander Hildebrandt, who encouraged me to become a PhD student.

Finally, I want to thank my family. I am grateful to Anita and Wolfgang for showing me how to always look at the positive side of things and never give up. You were great role models. I thank my parents for raising me with the belief that I can achieve whatever I want and for being proud of each and every one of my achievements. And I thank my partner Markus. Your love, support and belief in me have given me tremendous encouragement!

Contents

Part I

Overview

CHAPTER 1

Motivation and research objectives

Nickel-based superalloys are a class of high-strength, heat resistant materials. They are commonly used in applications that require materials operating in demanding environments with high mechanical loading and high temperatures, such as parts of gas turbines or jet engines. While parts like turbine blades are often made from single crystals, other parts like turbine disks are commonly made from polycrystalline material. When exposed to a combination of severe loading conditions including high temperatures, an oxygen-rich environment and sustained tensile loading, polycrystalline nickel-based superalloys are prone to crack initiation by environmentally assisted fatigue. The newly formed cracks can then in turn promote failure by other fracture mechanisms. This scenario has for example led to severely damaged jet engines in the past [1], [2], [3], [4], for the latter two examples technical investigations are detailed in [5] and [6]. A broken Inconel 718 turbine disk from the failure discussed in [2] is shown in Figure 1.1. The failure of the turbine disk caused an in-flight engine failure of a Boeing 767-219ER. The primary crack initiated on the left side and propagated inwards radially. The technical analysis of the turbine disk, conducted by the Australian Transport Safety Bureau, has found that the crack initiated by intergranular fatigue cracking, then transi-

Figure 1.1: Rear face of the broken stage-1 HPT disk from a Boeing 767-219ER (General Electric CF6-80A high-bypass turbofan engine). The fracture originated on the left side of the disk, the initial part of the crack broke intergranularly. Figure reprinted with permission from ATSB air safety investigation report 200205780 [2].

tioned to a mixed mode of intergranular fatigue and ductile overload, followed by crack propagation in progressive cyclic overload, before the missing part finally broke off in rapid ductile overload [2]. The measures for avoiding such types of failures focus on non-destructive crack detection during maintenance. However, in order to design parts which are less likely to experience environmentally assisted cracking, it is crucial to understand the chemo-mechanical fracture phenomenon underlying intergranular fatigue cracking and to make predictions under which conditions it is likely to occur, as well as to accurately describe ductile transgranular fracture.

Research objectives and limitations

Component design and, in view of the developments in the field of additive manufacturing, material design largely benefit from detailed understanding of and simulation tools for fracture mechanisms in nickel-based superalloys. So far, little modeling efforts have been focused on capturing the chemo-mechanical coupling in environmentally assisted intergranular fatigue cracking, which however is a well investigated phenomenon in experimental research

and is often caused by the presence of environmental oxygen. Capturing a more complete range of fracture processes in polycrystalline nickel-based superalloys further requires modeling of ductile transgranular fracture. The focus of this thesis lies on building models for capturing the material behavior on the grain scale. Ductile fracture models based on crystal plasticity can be found in literature, as well as ductile fracture models incorporating size-effects via gradient-enhanced plasticity models. However, there is a lack of models combining these two features, which are both crucial for accurately predicting the plastification preceding fracture, as well as the ductile fracture behavior of polycrystalline metals on the micro-scale.

The research objectives for this thesis are formulated as follows, where the first two objectives relate to modeling intergranular fracture in oxygen-rich environments and the last two objectives relate to modeling ductile transgranular fracture.

- Understand which factors influence environmentally assisted intergranular fracture in nickel-based superalloys and build a computational modeling framework for predictions of the interaction between environmental effects and the mechanical behavior of the grain structure.
- Extend the chemo-mechanical modeling framework in order to account for crack propagation along grain boundaries. Capture the dependence of intergranular crack propagation rates on different environmental and loading conditions, including varying dwell times and cyclic loading.
- Develop a modeling framework for ductile fracture in metals that accounts for microstructural dependence, such as size effects, the impact of crystal orientations and the geometry of the microstructure.
- Develop a model for transgranular crack propagation across grain boundaries in polycrystalline microstructures. The model needs to capture relevant micro-structural effects like how grain boundaries initially act as barriers to plastic slip and later degrade to allow for cracks to grow into the adjacent grain.

The overarching goal of this project is to develop numerical tools for damage and fracture in polycrystalline nickel-based superalloys on the micro-scale. Like in any project, it is crucial to impose limits on the scope of the work. For the presented thesis, these limits include focusing on pure trans- and

intergranular fracture, as well as excluding model parametrization and fatigue crack growth from the research scope.

CHAPTER 2

Introduction

Physical fracture phenomena in nickel-based superalloys

The turbine disk failure shown in Figure 1.1 is a typical example of the different fracture phenomena which can occur in nickel-based superalloys. At room temperature such materials predominantly fracture in a ductile transgranular manner. However, under specific loading conditions intergranular fracture can occur. Depending on the specific combination of conditions, the fracture mode can be influenced by local conditions, resulting in mixed trans- and intergranular fracture surfaces. Over the past decades, a significant amount of experimental work has been performed in order to understand the impact of the loading conditions and in particular of environmental oxygen on the fracture of nickel-based superalloys at high temperatures. This section gives a brief overview of experimental work that constitutes the basis for the chemo-mechanical modeling of oxygen-assisted intergranular fracture in this work. The experimental findings are summarized in the list below and translate into different aspects of the model presented in Paper A and Paper B.

1. Reduction of ultimate tensile strength
At high temperatures, a reduction of ultimate tensile strength and of ductility

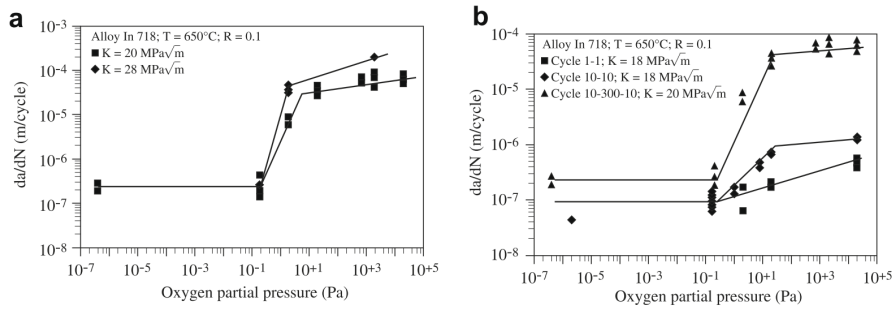

Figure 2.1: Crack propagation rates da/dN increase for increasing oxygen partial pressure in the environment. For higher oxygen partial pressures, a higher stress intensity factor leads to faster crack growth. The crack propagation is also accelerated for lower cyclic loading frequencies (compare the 1s-1s cycle to the 10s-10s cycle in b)). Figure reprinted from [10], page 2687, with permission from Elsevier, original results from [11].

is observed in oxygen-rich environments compared to those observed in vacuum. In particular, this effect occurs if the exposure to oxygen is combined with mechanical loading. Oxygen exposure without mechanical loading does not cause material degradation to the same degree. [7]

2. Acceleration of crack growth rate
At high temperatures, crack propagation is accelerated in oxygen-rich environments compared to vacuum. This effect is particularly pronounced when specimens are exposed to a dwell time in the oxygen-rich environment during tensile or cyclic loading [8], [9], [10].

3. Saturation of crack growth rate upon reaching a critical amount of oxygen
The acceleration of the crack growth rate in oxygen rich environments has been quantified in several experimental studies. The crack growth rates are found to depend on the environmental oxygen content [11], [9] and on the imposed dwell time [12], [8], [13], [14]. Examples illustrating these dependencies are shown in Figures 2.1 and 2.2, respectively.

The dependence of the crack growth rate on the environmental oxygen content is described in Figure 2.1 in terms of the oxygen partial pressure in the environment. The crack propagation per cycle is displayed for increasing oxy-

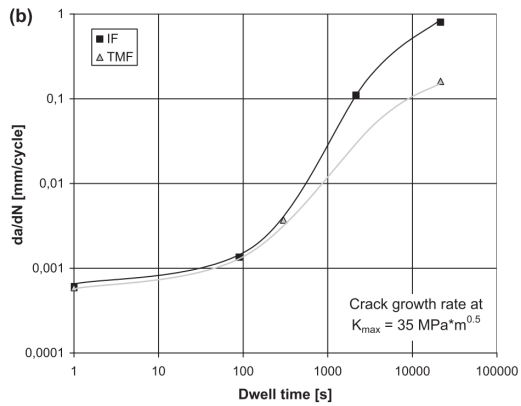

Figure 2.2: Crack propagation rates da/dN increase for longer dwell times at maximum load, both in isothermal fatigue (IF) and in thermo-mechanical fatigue (TMF). For very short and very long dwell times, saturation of the crack growth rate is observed. Figure reprinted from [13], page 8667, with permission from Elsevier.

gen partial pressure for different load levels, Figure 2.1a, and for varying dwell time, Figure 2.1b. It can be observed that the crack propagation rates are not dependent on low environmental oxygen concentrations. For increasing concentration, there is an oxygen range with quickly increasing crack growth rates around 1 Pa of oxygen partial pressure, followed by saturation of the crack propagation rates for high environmental oxygen concentrations. It is also important to notice that the cracks propagate intergranularly for high oxygen concentrations, but transgranularly for low oxygen concentrations. Mixed inter- and transgranular fracture occurs around 1 Pa oxygen partial pressure, where crack growth rates start to increase rapidly.

Furthermore, cracks propagate faster for higher loads and for longer dwell times. The latter is quantified in Figure 2.2 by showing the crack propagation per cycle for varying dwell times at the maximum load level. Similar to the dependence on oxygen pressure, short dwell times have a small impact on the crack growth rate, but with increasing dwell time, the cracks grow increasingly fast and for very long dwell times the crack propagation rate saturates. Similar to the behavior upon increasing oxygen concentrations, a transition

from transgranular crack growth for short dwell times to intergranular crack growth for long dwell times has been observed.

4. Presence of oxygen along grain boundaries only
Oxygen is found exclusively along grain boundaries and does not significantly diffuse into the grains [15], [16]. Notice that this is a major difference from hydrogen embrittlement where hydrogen diffusion into the bulk material is a relevant process.

To conclude from the experimental observations, the right sides of Figures 2.1 and 2.2 are related to intergranular fracture, while the left sides are related to transgranular fracture. Mixed trans- and intergranular fracture may occur in between. A critical amount of oxygen is needed for causing the transition from trans- to intergranular fracture, which is accompanied by an acceleration of crack growth. This critical amount of oxygen must be available from the environment in the first place (sufficiently high environmental oxygen content). Once available, there must be sufficient time for the critical amount of oxygen to enter into the structure, and in doing so oxygen can only travel along the grain boundaries. After the material has been damaged by oxygen, further increase of the oxygen concentration in the material does not affect the intergranular fracture process.

Intergranular crack growth in nickel-based superalloys is thus subject to specific loading conditions leading to the presence of oxygen in the grain boundaries. Under other conditions, for example at colder temperatures, in a vacuum or if there is no sustained dwell time under tensile loading during the loading cycles, nickel-based superalloys usually fracture transgranularly, see for example [11], [17], [16]. Crack surfaces for these different fracture modes are shown in Figure 2.3, which is reprinted from Hörnqvist *et al.* [16]. The specimen was pre-cracked in cyclic loading, first at room temperature and then at 700°C. Subsequently a sustained tensile load was applied at 700°C. Finally, the specimen was cooled down to room temperature and fully fractured by bending. The resulting fracture surface is shown in Figure 2.3a, where the crack has propagated from bottom to top. The crack front propagates transgranularly at room temperature and intergranularly at 700°C. The transitions from ductile transgranular fracture (room temperature) to brittle intergranular fracture (700°C) and vice versa can be seen in Figures 2.3c and 2.3d. Pure intergranular crack growth occurs during the sustained loading period, the corresponding fracture surface is shown in Figure 2.3b.

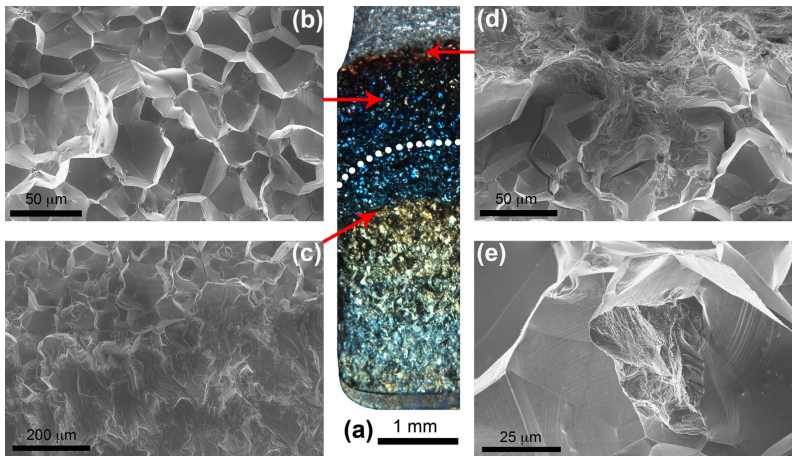

Figure 2.3: Example of a mixed trans- and intergranular crack surface. Subfigure (a) shows the sample, the crack front propagated from bottom to top. Subfigures (c) and (d) show transitions from ductile fracture at room temperature to intergranular fracture at 700°C and vice versa. A distinct intergranular fracture can be seen in Subfigure (b), which stems from crack propagation during a sustained tensile loading at 700°C. Subfigure (e) shows a remaining ligament in the intergranular crack surface that was broken off at room temperature. The example is reprinted from [16], page 135, with permission from Elsevier.

Numerical fracture modeling

In order to understand the fracture behavior of nickel-based superalloys on the grain scale, it is crucial to have models for both the intergranular and the transgranular fracture regimes. In terms of numerical fracture modeling, transgranular fracture is inherently different from intergranular fracture. In intergranular fracture possible crack paths are confined to a small subsection of the total domain, namely to the grain boundaries, while arbitrary fracture paths can occur in transgranular fracture. Various approaches to modeling material failure within the finite element method are present in the literature. They can generally be divided into discontinuous methods such as mesh splitting techniques, XFEM and cohesive zone modeling, and continuous methods such as (gradient-extended) continuum damage modeling and phase-field

modeling. In terms of discrete methods, cohesive zone modeling and mesh splitting techniques usually require either adaptive remeshing during the simulation or a priori knowledge of possible crack paths, while XFEM requires intricate shape function construction and can enlarge and significantly densify the stiffness matrix. Opposed to discontinuous methods which track discrete cracks, continuous methods use diffuse crack representations by introducing damage fields. They typically require a fine mesh discretization together with an increased number of degrees of freedom in the system. Based on the discussion in above, about the circumstances under which oxygen exposure leads to inter- instead of transgranular crack growth and based on the knowledge that oxygen is found only along grain boundaries, a chemo-mechanically coupled cohesive zone model for grain boundary fracture is developed in Paper A and Paper B.

Opposed to intergranular fracture, transgranular fracture can be considered the default fracture mode in nickel-based superalloys. It is also the fracture mode that leads to ductile fracture in many other polycrystalline metals, whereby the modeling of it is not specific to nickel-based superalloys. Ductile fracture of metals usually involves void nucleation and coalescence and/or instability in plastic shear bands. In these mechanisms, plasticity plays an important role [18]. In fatigue crack initiation, micro-crack development has also been shown to follow crystallographic directions [19]. On the grain scale, the mechanical behavior of each grain is anisotropic and dependent on its respective crystal orientations, which is typically modeled by crystal plasticity models. Various crystallographic phenomena can play into the formation of plasticity in metals, including plastic slip, twinning, diffusion of dislocations, grain boundary sliding, recrystallization and phase-transformations. Twinning is most relevant for materials with HCP crystal structure, diffusion mechanisms, grain boundary sliding, recrystallization and phase-transformations are associated with (extremely) high temperatures. Since nickel-based superalloys usually have a FCC crystal structure and the focus of this work regarding the high-temperature regime is oxygen-assisted fracture of the grain boundaries, the crystal plasticity model is here limited to plastic slip, although the viscoplastic regularization employed for uniqueness of the crystal plasticity model also allows for modeling of diffusion mechanisms. Plastic slip is caused by dislocation movement through the crystal lattice of the grains. Furthermore, metals have size-dependent stress-strain behavior on the micro-scale, which

in polycrystalline materials is largely attributed to the transmission and interaction of dislocations at interfaces. Grain boundaries are such interfaces and act as obstacles for slip transmission, as well as dislocation sinks. The degree of resistance that a particular grain boundary exhibits depends, among other things, on the slip system alignment of the respective grains [20]. This results in the Hall-Petch effect, where smaller grain sizes lead to a higher material strength. In the context of (crystal) plasticity models, this is typically modeled by strain gradient-extensions and grain boundary conditions.

Due to the arbitrary crack paths in transgranular fracture, as well as the relevance of obtaining a tight coupling between a gradient-enhanced crystal plasticity model and the fracture model, the approach chosen in this thesis is a continuous fracture method.

Continuum damage models depart from a diffuse fracture description, where the local stiffness in each material point is gradually reduced by one or more damage variables. The damage model then typically states some evolution law for the damage variable(s), usually in terms of the local strain energy. As long as the damage evolution is fully local, these models are known to suffer from mesh dependence. Possible ways to circumvent this problem include viscous- and gradient-regularization of the damage evolution law or the hardening stress, where especially gradient-regularizations are able to fully eliminate the mesh dependence. Gradient-damage models have in the past been a common choice for fracture modeling in combination with crystal plasticity models, see for example [21].

Phase-field modeling on the other hand is motivated by the variational formulation of Griffith's theory of brittle fracture. The core idea of phase field models is, again, to introduce a damage variable and use it for a diffuse representation of the fracture surfaces. Thereby, the integral over the fracture surfaces is replaced by a volume integral over a (diffuse) surface density function. The surface density function is a modeling choice, but suitable options must include the gradient of the damage variable. In phase-field models, a choice of degradation function must also be made, which describes how the stiffness degradation depends on the damage variable. Phase-field modeling gained interest in the fracture mechanics community in the context of brittle fracture [22], [23]. It has over the past decade proven to be a suitable modeling technique for a multitude of problems, including ductile fracture, see for example the comparison of ductile phase-field models by Alessi *et al.* [24].

Gradient-damage models and phase-field models, albeit having different motivations, share some ingredients: the stiffness degradation based on a damage variable, as well as a damage gradient regularization. While the approaches in their most common formulations are not the same, they can for simple base models like linear elasticity be cast into a common mathematical framework. In this case, the phase-field model can be formulated as a special case of a gradient-damage framework [25]. Due to the increasing popularity over the past decade phase-field modeling is chosen as continuous fracture modeling technique in Paper C and Paper D.

CHAPTER 3

Modeling

3.1 Chemo-mechanically coupled cohesive zone model

The oxygen-enhanced intergranular fracture mode, that can occur in nickel-based superalloys at high temperatures is sometimes also referred to as environmental fatigue. As discussed in Chapter 2, a combination of oxygen exposure and loading at high temperatures might lead to this fracture mode, and it is linked to sustained tensile loading rather than necessarily requiring cyclic loading, as classic fatigue does. However, sustained periods of tensile loading often occur during loading cycles of components like turbine disks.

This section introduces the chemo-mechanically coupled cohesive zone model presented in Paper A, as well as the extension of the modeling framework in order to account for crack propagation that is presented in Paper B. Cohesive zone modeling is used for representing the cracks, since the possible crack paths are a priori known. As it is also known that oxygen can only be transported along the grain boundaries, the oxygen concentration field is restricted to the grain boundary domain. An adaptation of the well known

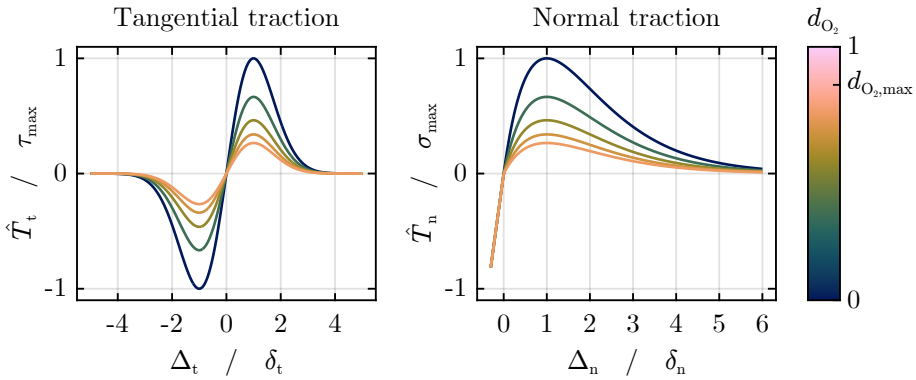

Figure 3.1: Environmental degradation of cohesive law. Initially, the strength of the cohesive law is τ_{max} in tangential and σ_{max} in normal direction. The maximum traction in each direction is reached when the respective jump Δ_t / Δ_n reaches its characteristic value δ_t / δ_n. For increasing environmental damage d_{O_2}, the tractions in normal and tangential direction decrease.

Xu-Needleman cohesive law [26] by Kolluri *et al.* [27] is employed as a base model for the mechanical behavior of the grain boundaries. In this section, an overview of the additions made to the base cohesive law in order to account for the chemo-mechanical phenomena discussed in Chapter 2 is given. For a complete model formulation, the reader is referred to the respective publications. The modeling framework results in a fully chemo-mechanically coupled model, meaning that the concentration field has an impact on the cohesive law, as well as that the cohesive law impacts the oxygen transport along the grain boundaries.

Environmental damage

The coupling between the concentration field on the grain boundaries c^{gb} and the cohesive law is realized by introducing a damage variable d_{O_2}. To account for the reduction of ultimate tensile strength and thereby giving rise to accelerated crack growth, the tractions resulting from the base cohesive law $\boldsymbol{T}^{base}$ are reduced by an environmental damage variable d_{O_2} such that

$$\hat{\boldsymbol{T}} = \left(1 - d_{O_2}\, \mathcal{H}\left(\Delta_n\right)\right) \boldsymbol{T}^{base}\,, \tag{3.1}$$

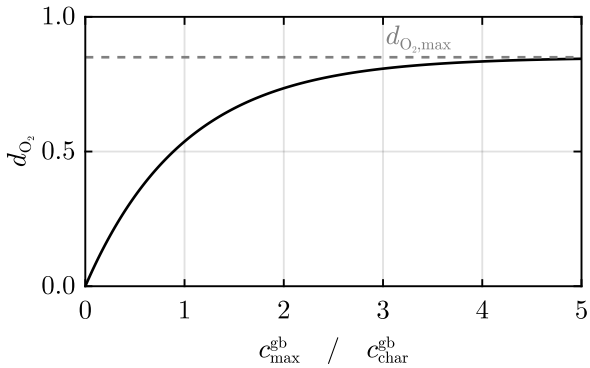

Figure 3.2: Relation between the environmental damage variable d_{O_2} and the maximum grain boundary concentration c^{gb}_{max}. The damage variable increases quickly around a characteristic oxygen concentration c^{gb}_{char}, which can be related to the regions of high crack rate acceleration in Figure 2.1.

where Δ_n is the normal displacement jump at the interface and $\mathcal{H}$ is the Heaviside function. The resulting tractions $\hat{\boldsymbol{T}}$ are represented in Figure 3.1. The strength of the cohesive law, and thus the fracture energy, is reduced upon increasing the environmental damage d_{O_2}. The reduction only happens for positive normal separation jumps $\Delta_n > 0$. Notice that the initial stiffness of the cohesive law is also reduced. This is a similar approach to the coupling between hydrogen concentration and fracture energy in hydrogen embrittlement, presented by Kristensen *et al.* [28]. Therein, the fracture energy of a phase-field model is degraded linearly with increasing hydrogen concentrations, which the authors base on quantum mechanical computations. Instead, the damage evolution is here motivated by the reports of saturating crack growth rates, compare Figures 2.1 and 2.2. The environmental damage is the main model feature for causing the accelerated crack growth rate. Therefore, the experimentally observed saturation effects in crack propagation rate enter the model at this point. The saturation effects are related to reaching a critical amount of oxygen in the grain boundaries, which is reflected by the saturation of the damage variable. The crack growth rate increases quickly around a characteristic oxygen concentration c^{gb}_{char} and saturates for much larger concentrations. In the model, this is accounted for by using an

exponential relation between the oxygen concentration and the environmental damage

$$d_{\mathrm{O}_2} = d_{\mathrm{O}_2,\max} \left(1 - \exp\left(-c^{\mathrm{gb}}_{\max} \,/\, c^{\mathrm{gb}}_{\mathrm{char}}\right)\right) , \tag{3.2}$$

where the history variable $c^{\mathrm{gb}}_{\max}$ has been introduced as maximum experienced oxygen concentration in a material point in order to ensure irreversibility. Additionally, an upper limit of the environmental damage $d_{\mathrm{O}_2,\max}$ is introduced as a model parameter, in order to control the level of damage that can be caused by the presence of oxygen. The relation between oxygen concentration and environmental damage is shown in Figure 3.2.

Stress-assisted oxygen diffusion

The second chemo-mechanical coupling reflects the impact of the mechanical state on the oxygen transport law. The base assumption for oxygen transport into the structure is that oxygen diffuses along the grain boundaries. This is accounted for by a diffusive oxygen flux $\boldsymbol{j}^{\mathrm{gb}}_{\mathrm{chem}}$ according to Fick's law. Additionally, it is known that accelerated crack growth is associated with oxygen exposure under mechanical loading. In order to account for this, the assumption of stress-assisted diffusion towards high hydro-static stresses (originally suggested by Sofronis and McMeeking [29] in the context of hydrogen embrittlement) is adopted. As the hydro-static stress is not readily available in cohesive elements, the mechanically assisted flux $\boldsymbol{j}^{\mathrm{gb}}_{\mathrm{mech}}$ is instead assumed to be proportional to the gradient of normal traction $\boldsymbol{\nabla}^{\mathrm{gb}}\hat{T}_{\mathrm{n}}$. The oxygen flow in the grain boundaries $\boldsymbol{j}^{\mathrm{gb}}$ can then be expressed as

$$\boldsymbol{j}^{\mathrm{gb}} = \underbrace{-\,D\,\boldsymbol{\nabla}^{\mathrm{gb}} c^{\mathrm{gb}}}_{\boldsymbol{j}^{\mathrm{gb}}_{\mathrm{chem}}} + \underbrace{D\,c^{\mathrm{gb}}\,\frac{V_{\mathrm{O}_2}}{\mathrm{R}\,T}\,\boldsymbol{\nabla}^{\mathrm{gb}}\hat{T}_{\mathrm{n}}}_{\boldsymbol{j}^{\mathrm{gb}}_{\mathrm{mech}}} . \tag{3.3}$$

Therein, the introduced model parameters are the base diffusivity along grain boundaries D and the partial molar volume of oxygen in metal V_{O_2}. Furthermore, R is the universal gas constant and T is the absolute temperature. In the damage zone, the mechanical flux $\boldsymbol{j}^{\mathrm{gb}}_{\mathrm{mech}}$ is the dominant phenomenon transporting oxygen along the grain boundaries, thus ensuring that significantly less oxygen can enter the structure without mechanical loading ($\boldsymbol{\nabla}^{\mathrm{gb}}\hat{T}_{\mathrm{n}} = \boldsymbol{0}$). However, the chemical flux $\boldsymbol{j}^{\mathrm{gb}}_{\mathrm{chem}}$ plays an important role in the initiation of the degradation process, as it is the first phenomenon bringing small amounts

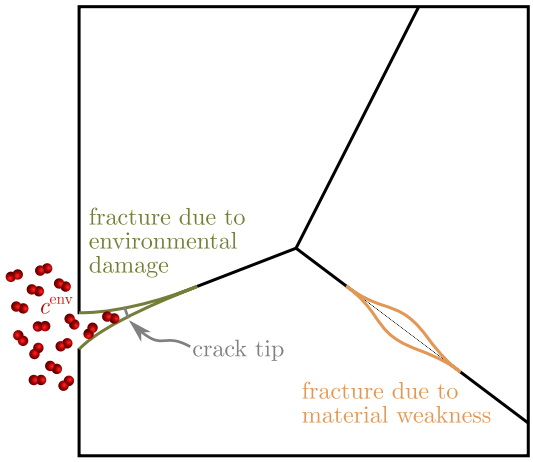

Figure 3.3: Different fracture scenarios: Edge cracks (green / left) should fill up with oxygen, while interior cracks (orange / right) should not. Figure reprinted from Paper B.

of oxygen into the structure. The oxygen starts to degrade the cohesive law according to Equation (3.1), resulting in increasing traction gradients between regions with and without oxygen. This in turn gives rise to the traction assisted oxygen flux $\boldsymbol{j}^{\text{gb}}_{\text{mech}}$.

Moving boundary condition

In the next step, the modeling framework is employed for computing crack propagation rates in polycrystals. When modeling the propagation of cracks that originate on external boundaries, it is crucial to discuss the evolution of the oxygen boundary condition. Figure 3.3 visualizes different crack types and their relation to the environmental boundary condition. To the left, it shows an edge crack, that opens up to the environmental oxygen supply. The oxygen concentration in the environment is typically much larger than the critical oxygen concentration needed for degrading the mechanical response of the grain boundaries. The chemo-mechanically coupled model presented in Paper A describes the oxygen flux *ahead* of the crack tip, but does not accurately depict what happens *behind* the crack tip. For cracks that open up towards the domain boundary, it is assumed that oxygen transport from the

boundary into the (open) crack is much faster than the oxygen transport in the grain boundaries. This corresponds to assuming that the environmental medium, for example air, instantaneously flows from the environment into the crack. Thus, the crack flanks which open towards the domain boundary should be exposed to the environmental oxygen concentration as soon as the crack grows. It is important to capture this correctly, in order to ensure meaningful concentration gradients as input to the chemo-mechanically coupled model. because oxygen transport in the grain boundaries is a much slower process than oxygen flow from the environment into broken grain boundaries.

Several advanced boundary conditions on the concentration field in chemo-mechanically coupled problems can be found in literature, for example hydrostatic stress dependent boundary conditions for hydrogen embrittlement in [30] and [31] or boundary conditions on oxygen flux motivated by oxidation kinematics [32], [33]. An approach that tackles the problem of evolving crack fronts described above has been employed by Kristensen *et al.* [28] and Golahmar *et al.* [34]. Therein, the difference between the environmental oxygen concentration and the local oxygen concentration is penalized in broken material points. Their work employs a phase-field fracture model and broken material points are identified by the value of the scalar phase-field. While this approach shows promising results, it suffers a severe drawback in the context of complex crack patterns: Consider a crack that initiates inside the structure instead of on the domain boundary, as visualized on the right of Figure 3.3. This crack is not connected to the oxygen supply and should therefore not be filled up with oxygen, which is disobeyed in the case of penalizing the concentration field.

In order to solve this problem, another penalty approach is proposed in Paper B, which instead penalizes the concentration gradient $\boldsymbol{\nabla}^{\mathrm{gb}} c^{\mathrm{gb}}$ in the broken regions. Combined with Dirichlet boundary conditions on the concentration field at the outer boundary of the structure, this approach enforces the concentration inside edge cracks to be equal to the environmental oxygen concentration, since spatial changes of the concentration are penalized wherever the grain boundaries are broken. On the other hand, for a crack unconnected to the boundary, the only effect is a constant concentration throughout the crack.

The penalty condition is imposed by adding a penalty term to the weak form of the mass conservation of oxygen, such that the virtual work is extended by

a term related to the boundary condition $\delta\mathcal{W}^{\mathrm{bc}}$

$$\delta \mathrm{W}^{\mathrm{bc}} = p_{\mathrm{bc}} \int_{\Gamma_{\mathrm{f}}} \boldsymbol{\nabla}^{\mathrm{gb}} c^{\mathrm{gb}} \cdot \boldsymbol{\nabla}^{\mathrm{gb}} \delta c^{\mathrm{mid}} \, \mathrm{d}A \,, \tag{3.4}$$

where p_{bc} is a penalty coefficient, δc^{mid} is the test function for the concentration field and Γ_{f} are the broken grain boundaries.

There are several damage variables in the employed cohesive zone model, whereby a scalar criterion for determining the broken domain Γ_{f} needs to be defined. Since the model is built on a cohesive law with a strong coupling between the normal and tangential directions, the fracture criterion is here based solely on the remaining normal strength T_{r}. A material point is considered broken once the remaining normal strength falls below a limit traction value for fracture T_{f}, such that the domain of fractured grain boundaries Γ_{f} is defined as

$$\Gamma_{\mathrm{f}} = \{ \boldsymbol{X} \in \Gamma_{\mathrm{s}} : \; T_{\mathrm{r}} \leq T_{\mathrm{f}} \} \,. \tag{3.5}$$

Therein, Γ_{s} is the total grain boundary domain. For a more detailed explanation of the fracture criterion, the reader is referred to Paper B. The fracture criterion can then be employed to reformulate Equation 3.4 as an integral over the entire grain boundary domain

$$\delta \mathrm{W}^{\mathrm{bc}} = p_{\mathrm{bc}} \int_{\Gamma_{\mathrm{s}}} \mathcal{H} \left(T_{\mathrm{f}} - T_{\mathrm{r}} \right) \boldsymbol{\nabla}^{\mathrm{gb}} c^{\mathrm{gb}} \cdot \boldsymbol{\nabla}^{\mathrm{gb}} \delta c^{\mathrm{mid}} \, \mathrm{d}A \,. \tag{3.6}$$

Notice that the penalty term can also be interpreted as an additional oxygen flux due to the moving boundary condition $\boldsymbol{j}_{\mathrm{bc}}^{\mathrm{gb}}$. This consideration reveals a problem with implementing Equation 3.6: The oxygen flux resulting from the moving boundary condition is very large compared to the chemical and mechanical fluxes transporting oxygen ahead of the crack tip. Subjecting the presence of this flux to a discrete Heaviside function, and thereby drastically changing the oxygen diffusivity from one integration point to the next, results in numerical problems. The boundary condition in that case behaves like a shock wave. In order to alleviate this problem, a regularized Heaviside function is applied to the fracture criterion instead. However, the remaining normal strength T_{r} itself also has very steep gradients close to the crack tip, which limits the possibility to use it for regularization. Therefore, an additional regularization driven by the normal jump has been introduced as well. Furthermore, the boundary flux should be a strictly trailing phenomenon to

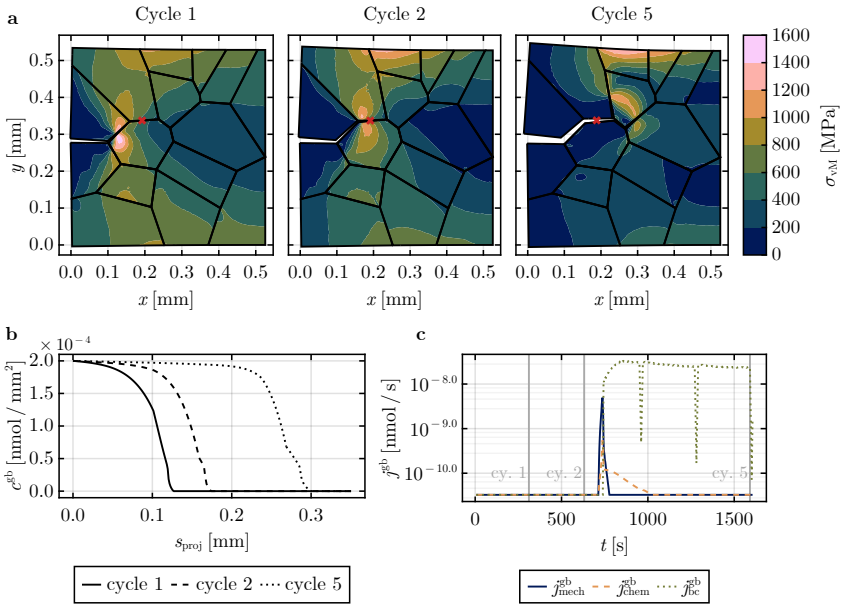

Figure 3.4: Example of intergranular crack propagation under consideration of the moving oxygen boundary condition. The contour plots in Subfigure a show three snapshots of the von Mises stresses during cyclic loading. Subfigure b shows the oxygen concentrations along the crack path. Subfigure c shows the three oxygen transport mechanisms for the point marked with a red cross on top. Figure reprinted from Paper B, page 5192.

the fracture process and only interact with the coupled cohesive zone model in terms of supplying realistic conditions behind the crack tip. In particular, the oxygen flux caused by the moving boundary condition should not be larger than the chemical or mechanical flux ahead of the crack tip. This needs to be considered when formulating the regularizations. In Paper B the regularized Heaviside function is therefore modified such that the effective diffusivity for the boundary flux never exceeds a tolerated limit value for a given remaining strength.

Numerical example

Figure 3.4 shows a simulation result where the chemo-mechanically coupled cohesive zone law presented in Paper A is combined with the moving oxygen boundary condition presented in Paper B. Figure 3.4a shows three snapshots of the von Mises stresses during the cyclic loading. The crack tip in each of the snapshots can be identified by the stress concentrations. Figure 3.4b shows the oxygen concentrations along the crack at the same three time snapshots. The oxygen concentration in the broken section of the crack is close to the environmental oxygen concentration. As the crack propagates, the section of the grain boundaries experiencing the environmental oxygen concentration propagates along with it. Figure 3.4c shows the sequence of the different oxygen transport mechanisms for the point marked with a red cross in Figure 3.4a. No oxygen transport occurs while the crack tip is far away from the point. Comparing with Figure 3.4b, it becomes clear that the material point does not have any oxygen exposure before it is reached by the crack tip. When the crack tip approaches, the chemical $j^{\mathrm{gb}}_{\mathrm{chem}}$ and the mechanical oxygen flux $j^{\mathrm{gb}}_{\mathrm{mech}}$ increase first. This is when the coupled model from Paper A determines the material behavior. After the material point breaks, oxygen flows in from the environment and the oxygen concentration is determined by the moving boundary condition $j^{\mathrm{gb}}_{\mathrm{bc}}$ presented in Paper B.

3.2 Ductile phase-field fracture model

After damage initiation by environmentally assisted fatigue, polycrystalline nickel-based superalloys often fail by ductile transgranular fracture. In this case the crack path is not known and strongly depends on the mechanical state, as well as the material and its microstructure. The second part of this thesis focuses on the modeling of transgranular ductile failure by phase-field modeling, aiming to capture the mechanical behavior of metallic polycrystalline microstructures. In Paper C and Paper D, a thermodynamically consistent modeling framework combining gradient crystal plasticity and phase-field fracture was developed and employed to polycrystals. The model is derived from a free energy Ψ

$$\Psi = \underbrace{g_{\mathrm{e}}\left(d,\, \epsilon^{\mathrm{p}}\right)}_{\substack{\text{degradation}\\ \text{function}}} \underbrace{\hat{\Psi}_{\mathrm{e}}\left(\boldsymbol{C}_{\mathrm{e}}\right)}_{\substack{\text{hyper-}\\ \text{elasticity}}} + \underbrace{\hat{\Psi}_{\mathrm{p}}\left(\{k_\alpha\}_{\alpha=1}^{n_\alpha},\, \{\boldsymbol{\nabla}_0 k_\alpha\}_{\alpha=1}^{n_\alpha}\right)}_{\substack{\text{gradient-enhanced}\\ \text{crystal plasticity}}} + \underbrace{\Psi_{\mathrm{d}}\left(d, \boldsymbol{\nabla}_0 d\right)}_{\substack{\text{phase-field}\\ \text{model}}}, \quad (3.7)$$

where, $\hat{\Psi}_{\mathrm{e}}$, $\hat{\Psi}_{\mathrm{p}}$ and Ψ_{d} are the respective free energy formulations for hyper-elasticity, the gradient-enhanced crystal plasticity model and the phase-field models. The elastic degradation function g_{e} represents the coupling between the phase-field model and the elasto-plastic base model. The chosen algorithmic framework introduces three different fields: The displacement field $\boldsymbol{u}$, from which the right Cauchy-Green deformation tensor $\boldsymbol{C}_{\mathrm{e}}$ is computed, a gradient field $\boldsymbol{g}$, which relates to the gradient of the plastic hardening variables $\{k_\alpha\}_{\alpha=1}^{n_\alpha}$ and the phase-field damage d. An additional local variable ϵ^{p} is a scalar representation of accumulated plastic strain. While Paper D employs the same modeling framework as Paper C, the prototype models differ in some of their modeling choices. In this chapter insights into chosen model features are given. For a full description the reader is referred to Paper C and Paper D.

Ductile phase-field modeling

The phase-field models in both articles employ a classical AT2-surface energy functional, such that

$$\Psi_{\mathrm{d}}\left(d, \boldsymbol{\nabla}_0 d\right) = \mathcal{G}_0^{\mathrm{d}}\, \Gamma_{\mathrm{d}}\left(d, \boldsymbol{\nabla}_0 d\right) \quad \text{with } \Gamma_{\mathrm{d}} = \frac{1}{2\,\ell_0}\left(d^2 + \ell_0^2\,|\boldsymbol{\nabla}_0 d|^2\right) . \tag{3.8}$$

Therein, $\mathcal{G}_0^{\mathrm{d}}$ is the fracture toughness and ℓ_0 is the characteristic length scale associated with the phase-field model. Coupled to elasticity, the AT2 surface energy functional leads to brittle failure. Various ductile phase-field models that couple the AT2 surface energy functional to elasto-plastic material behavior are present in the literature. Two approaches to achieving a ductile fracture response are dominant in these models: The first approach imposes degradation functions on the elastic and the plastic free energy contributions and the second approach incorporates a plastic variable in the degradation function.

A free energy formulation for the first approach takes the form

$$\Psi = g_{\mathrm{e}}\left(d\right)\hat{\Psi}_{\mathrm{e}} + g_{\mathrm{p}}\left(d\right)\hat{\Psi}_{\mathrm{p}} + \Psi_{\mathrm{d}}\left(d,\, \boldsymbol{\nabla}_0 d\right) , \tag{3.9}$$

where g_{e} and g_{p} are the degradation functions associated with the elastic and plastic free energy contributions $\hat{\Psi}_{\mathrm{e}}$ and $\hat{\Psi}_{\mathrm{p}}$, respectively. The corresponding phase-field equation, when considering the AT2 surface energy functional, is

then derived as

$$-\frac{\partial g_{\mathrm{e}}}{\partial d}\hat{\Psi}_{\mathrm{e}} - \frac{\partial g_{\mathrm{p}}}{\partial d}\hat{\Psi}_{\mathrm{p}} - \frac{\mathcal{G}_0^{\mathrm{d}}}{\ell_0}d + \mathcal{G}_0^{\mathrm{d}}\ell_0 \boldsymbol{\nabla}_0 \cdot \boldsymbol{\nabla}_0 d = 0 \tag{3.10}$$

It can be seen that the damage evolution in this formulation is driven by both elastic and plastic strain energy. Often, the same degradation function is adopted for the elastic and plastic contributions. This approach in combination with the common quadratic degradation function $g_{\mathrm{e}} = g_{\mathrm{p}} = (1-d)^2$ has for example been adopted by Kuhn *et al.* [35] and Miehe *et al.* [36], even though the latter employs a more complex extension of the AT2 model. Damage initiation in this case starts in the same manner as for the elastic AT2 phase-field model in the elastic zone, causing a non-linear response from the beginning. Therefore, cubic degradation functions, which can produce a linear elastic initial response, are employed for example by Borden *et al.* [37] and Maloth and Ghosh [38] in the same context. Notice however, that even with a cubic degradation function there is no guarantee for retaining the original elastic response built into the model.

The second approach incorporates a plastic strain measure in the degradation function and applies the degradation function only to the elastic free energy contribution, as shown in Equation (3.7) [39]. The ductile fracture behavior is then realized via the choice of degradation function g_{e}. The degradation function affects the mechanical stiffness via the computation of the second Piola-Kirchhoff stress tensor $\boldsymbol{S}_{\mathrm{e}}$

$$\boldsymbol{S}_{\mathrm{e}} = 2\,\frac{\partial \Psi}{\partial \boldsymbol{C}_{\mathrm{e}}} = 2\,g_{\mathrm{e}}\left(d,\,\epsilon^{\mathrm{p}}\right)\,\frac{\partial \hat{\Psi}_{\mathrm{e}}}{\partial \boldsymbol{C}_{\mathrm{e}}}\,, \tag{3.11}$$

and also plays a role in the computation of the phase-field damage d via the phase-field equation, which when considering an AT2 surface energy functional is derived as

$$-\frac{\partial g_{\mathrm{e}}}{\partial d}\hat{\Psi}_{\mathrm{e}} - \frac{\mathcal{G}_0^{\mathrm{d}}}{\ell_0}d + \mathcal{G}_0^{\mathrm{d}}\ell_0 \boldsymbol{\nabla}_0 \cdot \boldsymbol{\nabla}_0 d = 0\,. \tag{3.12}$$

A ductile degradation function for this approach has been suggested by Ambati *et al.* [39]. The degradation function depends on a measure of accumulated plastic strain ϵ^{p}, as well as the phase field damage d

$$g_{\mathrm{e}} = (1-d)^{2\left(\epsilon^{\mathrm{p}}\,/\,\epsilon^{\mathrm{p}}_{\mathrm{char}}\right)^{n}}\,, \tag{3.13}$$

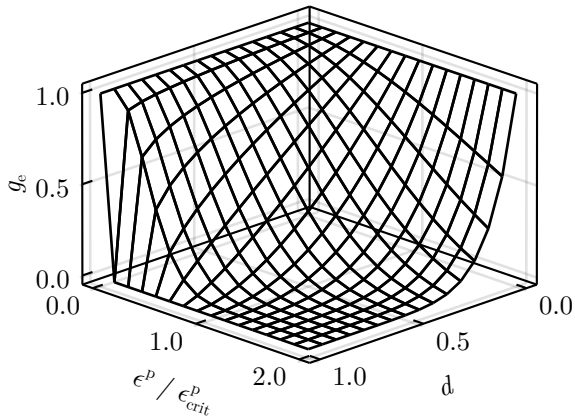

Figure 3.5: The degradation function g_e depends on the accumulated plastic strain ϵ^P, as well as the phase-field damage d. Material degradation can only occur in the presence of plastification and damage.

where ϵ^P_{char} is introduced as a characteristic value of the accumulated plastic strain, and n is a parameter determining the rate of material degradation. This degradation function is visualized in Figure 3.5. Its major characteristic is that material degradation only occurs for a combination of non-zero plastic strain and non-zero phase-field damage. An important property is that it retains the original elastic behavior in the elastic regime. In an undamaged material where $d = 0$ for all points and thus $\boldsymbol{\nabla}_0 \cdot \boldsymbol{\nabla}_0 d = 0$, damage can only start to develop for non-zero derivatives of the degradation function (compare Equation (3.12)). The derivative $\partial g_e / \partial d$ however remains zero as long as $\epsilon^P = 0$, whereby damage development in the elastic range is impossible for undamaged material. Since ductile damage in metals is usually preceded by significant plastification, the built-in nature of this mechanism in the Ambati degradation function is a compelling choice and this is the approach that has been pursued in this work.

Damage irreversibility

Phase-field models require an explicit handling of damage irreversibility in order to avoid material healing upon unloading. Classical ways of implementing this include for example the so-called history variable approach [23] or constraint optimization techniques, for different approaches see for example [40], [41], [42].

The history variable approach introduces a history variable $\mathcal{H}_\mathrm{e}$ for the maximum (elastic) strain energy that has occurred until the current time t, such that

$$\mathcal{H}_\mathrm{e} = \max_{\tilde{t} \leq t} \hat{\Psi}_\mathrm{e} \,. \tag{3.14}$$

The phase-field equation, Equation (3.12), thereby becomes

$$-\frac{\partial g_\mathrm{e}}{\partial d}\mathcal{H}_\mathrm{e} - \frac{\mathcal{G}_0^\mathrm{d}}{\ell_0} d + \mathcal{G}_0^\mathrm{d} \ell_0 \boldsymbol{\nabla}_0 \cdot \boldsymbol{\nabla}_0 d = 0 \,. \tag{3.15}$$

Since the strain energy is the driving factor behind the growth of the damage variable in this equation, the damage is constrained to increase by the introduction of the damage variable. This transformation, however, results in the loss of variational consistency, see for example [43]. Similar history variable(s) can also be formulated for the class of ductile phase-field models represented by Equation (3.9).

Micromorphic approaches [44] have occasionally been employed in phase-field modeling, for example in [45] in order to enhance the numerical robustness. Recently, Bharali *et al.* [46] proposed to employ a micromorphic approach for implementing damage irreversibility. Contrary to the history variable approach, this results in a both thermodynamically and variationally consistent formulation. The micromorphic framework introduces an additional *local* damage variable φ, which is tied to the global phase-field damage d via a penalty term with the penalty parameter α. The free energy is then modified compared to Equation (3.7) such that

$$\Psi = g_\mathrm{e}\left(\varphi,\, \epsilon^\mathrm{p}\right) \hat{\Psi}_\mathrm{e} + \hat{\Psi}_\mathrm{p} + \Psi_\mathrm{d}\left(\varphi, \boldsymbol{\nabla}_0 d\right) + \frac{\alpha}{2}\left(\varphi - d\right)^2 \,. \tag{3.16}$$

Since two thermodynamic variables, φ and d, relate to the phase-field formulation in this case, two corresponding phase-field equations are obtained from this formulation. Assuming an underlying AT2 surface energy functional like

above, the phase-field associated strong form, which is solved on the global level, becomes

$$\alpha\,(\varphi - d) + \mathcal{G}_0^{\mathrm{d}}\,\ell_0\,\boldsymbol{\nabla}_0 \cdot \boldsymbol{\nabla}_0 d = 0\,. \tag{3.17}$$

Additionally, a local equation is obtained

$$-\frac{\partial g_{\mathrm{e}}}{\partial \varphi}\,\hat{\Psi}_{\mathrm{e}} - \frac{\mathcal{G}_0^{\mathrm{d}}}{\ell_0}\,\varphi - \alpha\;(\varphi - d) = 0\,. \tag{3.18}$$

A trial value for the local damage φ^{trial} is obtained from solving the local phase-field equation. The trial value is then compared to the local damage value from the previous time step φ^{old} and the current local damage is determined such that $\varphi = \max\left(\varphi^{\mathrm{trial}},\, \varphi^{\mathrm{old}}\right)$. Note that this formulations leads to a somewhat more non-linear phase-field formulation compared to the history variable approach. This can easily be seen in the case of linear elasticity paired with a quadratic degradation function. A staggered solver step solving the global phase-field equation always results in solving a linear system for Equation (3.15), but might result in a non-linear system for Equation (3.17). Bharali *et al.* have presented the micromorphic irreversibility criterion within a small strain, linear elasticity framework. In Paper C, the formulation has been adopted for the proposed gradient-enhanced crystal plasticity based, finite strain framework. The micromorphic irreversibility criterion has shown to perform well on the ductile phase-field model, thus the formulation is kept for the prototype model in Paper D.

Gradient-enhanced crystal plasticity

While a variety of ductile phase-field models has been presented in literature, there is a lack of models that incorporate features on the grain scale, which are needed for an accurate description of microstructural damage initiation and fracture. Namely, a combination of crystal plasticity with a gradient-enhanced hardening extension is necessary in order to capture the crystal orientation dependent response in the different grains, as well as the size dependence observed for metals. Ductile phase-field models coupled to crystal plasticity can be found in literature, see [47], [38], as well as phase-field models considering gradient-extended hardening, for example [48], [28]. In Paper C, a phase-field fracture model incorporating gradient-enhanced crystal plasticity is presented for single crystals and extended to polycrystals in Paper D.

Gradient hardening can be interpreted as a modification of the yield limit based on a strain gradient measure. It affects the yield functions for the slip systems Φ_α via the hardening stresses κ_α

$$\Phi_\alpha = |\hat{\tau}_\alpha| - (\tau_\mathrm{y} + \kappa_\alpha) \,, \tag{3.19}$$

with $\hat{\tau}_\alpha = \tau_\alpha \,/\, g_\mathrm{e}\,(d,\, \epsilon^\mathrm{p})$, wherein τ_α is the standard crystal plasticity Schmid stress and τ_y is the yield limit on each slip system. The hardening stresses κ_α include contributions for isotropic hardening and gradient hardening. In Paper C, the hardening stresses are given by

$$\kappa_\alpha = \underbrace{-H_\alpha\, k_\alpha}_{\text{isotropic hardening}} \underbrace{+ H_\alpha^\mathrm{g}\, l_\mathrm{g}^2\, \bar{\boldsymbol{s}}_\alpha \cdot (\boldsymbol{\nabla}_0 \otimes \boldsymbol{\nabla}_0 k_\alpha) \cdot \bar{\boldsymbol{s}}_\alpha}_{\text{gradient hardening}} \,, \tag{3.20}$$

where subindex α refers to the slip system number, n_α is the number of slip systems in total, H_α is the isotropic hardening modulus, l_g is the length scale relating to gradient hardening, H_α^g is the gradient hardening modulus and $\bar{\boldsymbol{s}}_\alpha$ is the slip direction. Since Equation (3.20) includes gradients of the isotropic hardening variables, it becomes obvious that it cannot be solved locally in the material points and requires an additional global equation. Typically this is approached either by primal or by dual formulations [49]. In a primal formulation, the hardening variables are introduced as global fields and for example the yield function is employed as global strong form. However, including the yield function on the global level might require an active set search for the plastifying subdomain during the global solution procedure. Dual formulations on the other hand introduce the gradient of the hardening variables as fields and introduce the equality between the gradient fields and the gradients of the hardening variables as field equations. The dual approach is pursued in Paper C and Paper D, however employing slightly different gradient hardening formulations. In Paper C, a vector field $\boldsymbol{g}_\alpha$ is introduced for each slip system, $\boldsymbol{g}_\alpha = \boldsymbol{\nabla}_0 k_\alpha$, resulting in a set of α global weak forms

$$\delta W_\alpha^\mathrm{g} = \int_{V_0} \boldsymbol{g}_\alpha \cdot \delta \boldsymbol{g}_\alpha \,\mathrm{d}V_0 + \int_{V_0} k_\alpha\, \boldsymbol{\nabla}_0 \cdot \delta \boldsymbol{g}_\alpha \,\mathrm{d}V_0 - \int_{\partial V_0} k_\alpha\, \boldsymbol{N} \cdot \delta \boldsymbol{g}_\alpha \,\mathrm{d}A_0 \,, \tag{3.21}$$

where V_0 represents the initial domain with boundary ∂V_0. Thereby, Equation (3.20) can be solved in the manner of a standard plasticity model again, where $\boldsymbol{\nabla}_0 \otimes \boldsymbol{g}_\alpha$ is an input to the local material routine. The dual approach has also been shown to be numerically robust [50], [49].

The dual formulation chosen in Paper C introduces a full vector field per slip system. For the FCC crystal structure, which is common for many nickel-based superalloys, this results in 12 additional vector fields and quickly generates very computationally expensive problems. In this particular case, it would have been possible to introduce scalar fields $g_\alpha = \boldsymbol{\nabla}_0 k_\alpha \cdot \bar{\boldsymbol{s}}_\alpha$, which is computationally cheaper than vector fields, but still expensive when adopting larger problems. Therefore, the gradient hardening formulation has been altered in Paper D, where the hardening stresses are given by

$$\kappa_\alpha = -H_\alpha \, k_\alpha + H^{\mathrm{g}} \, l_{\mathrm{g}}^2 \sum_{\beta=1}^{n_\alpha} (\boldsymbol{\nabla}_0 \cdot \boldsymbol{\nabla}_0 k_\beta) \; . \tag{3.22}$$

In this formulation, gradient hardening is considered isotropic across all slip systems, that is the gradient of the hardening variable in one slip system affects the gradient hardening stresses in all slip systems. This is clearly a simplification of the physics, but allows to introduce a single vector field for gradient hardening $\boldsymbol{g} = \sum_{\alpha=1}^{n_\alpha} \boldsymbol{\nabla}_0 k_\alpha$. The corresponding weak form thus reads

$$\begin{aligned} \delta \mathcal{W}_i^g = \int_{V_{0,i}} \boldsymbol{g} \cdot \delta \boldsymbol{g} \, \mathrm{d}V_0 + \int_{V_{0,i}} \sum_{\alpha=1}^{n_\alpha} k_\alpha \, \boldsymbol{\nabla}_0 \cdot \delta \boldsymbol{g} \, \mathrm{d}V_0 \\ - \int_{A_{0,i}} \sum_{\alpha=1}^{n_\alpha} k_\alpha \, \boldsymbol{N} \cdot \delta \boldsymbol{g} \, \mathrm{d}A_0 \, , \end{aligned} \tag{3.23}$$

where $V_{0,i}$ represents the i-th grain with boundary $\partial V_{0,i}$. Simplifying the gradient hardening model has further advantages when it comes to boundary conditions for the gradient hardening field(s). Gradient hardening represents the dislocation densities in the crystal lattice, that is described by slip directions and slip normals. Since the slip systems are local to each grain, the gradient hardening field is in Paper D also assumed to be local to the grains, meaning it is discontinuous across the grain boundaries of a polycrystal. This results in the (mathematical) need to define boundary conditions on the grain boundaries. Additionally, the size effects that are captured by the gradient-enhanced plasticity model are, in particular in polycrystals, closely associated with the boundary conditions on the grain boundaries, since these represent the resistance of the grain boundaries to slip transmission. Thermodynamic consistency implies the following requirement for the boundary conditions in

a polycrystal with n_{grains} grains in total

$$\sum_{i=1}^{n_{\text{grains}}} \int_{\partial V_{0,i}} \left(-H^g \, l_g^2 \, \boldsymbol{N} \cdot \boldsymbol{g}\right) \sum_{\alpha=1}^{n_\alpha} \dot{k}_\alpha \, \mathrm{d}A_0 \geq 0 \,. \tag{3.24}$$

This inequality can trivially be fulfilled, yielding the two most commonly used boundary conditions:

1. **Micro-free boundary conditions**. $\boldsymbol{N} \cdot \boldsymbol{g} = 0$, which can be implemented by Dirichlet-type constraints in the dual formulation. This means that the gradient of the hardening variables needs to be parallel to the boundary on the grain boundaries.

2. **Micro-hard boundary conditions**. $\sum_{\alpha=1}^{n_\alpha} k_\alpha = 0$, whereby also $\sum_{\alpha=1}^{n_\alpha} \dot{k}_\alpha = 0$, which can be implemented by Neumann boundary conditions in the dual formulation, compare Equation (3.23). This means that no plastification can occur on the grain boundaries.

In terms of plastic slip transmission resistance, micro-free boundary conditions represent the case of no resistance against dislocation transmission, while micro-hard boundary conditions represent the case of complete resistance against plastic slip transmission. Both cases lack the capability to represent certain physical phenomena. While micro-free boundary conditions cannot represent the Hall-Petch effect, micro-hard boundary conditions prevent the formation of any plastic strain on the grain boundary. Recapitulating the properties of the adopted degradation function, compare Figure (3.5), this also means that the material then cannot degrade on the grain boundaries. Thus micro-hard boundary conditions prevent crack propagation across grain boundaries. Ekh *et al.* [51] have presented so-called micro-flexible boundary conditions which allow a smooth transition between micro-free and micro-hard boundary conditions, including in-between states where grain boundaries exhibit some, but not complete resistance to slip transmission. Micro-flexible boundary conditions, similar to micro-hard boundary conditions employ the boundary term in Equation (3.23) in order to prescribe the sum of the hardening variables $\sum_{\alpha=1}^{n_\alpha} k_\alpha$ on the grain boundaries

$$\sum_{\alpha=1}^{n_\alpha} k_\alpha = \left(-H^{\mathrm{g}} \, l_{\mathrm{g}}^2 \boldsymbol{N} \cdot \boldsymbol{g}\right) \, C_\Gamma \,, \tag{3.25}$$

where C_Γ is a micro-flexibility parameter controlling if the boundary tends more towards micro-free or micro-hard behavior. For $C_\Gamma \to 0$, micro-hard boundary conditions are recovered and for $C_\Gamma \to \infty$ it is required that $\boldsymbol{N} \cdot \boldsymbol{g} = 0$, thus recovering micro-free boundary conditions. This micro-flexibility parameter is used in Paper D to to obtain grain boundary behavior that has expressed micro-hard properties in the hardening range, but turns towards micro-free grain boundary behavior in the softening range in order to let cracks propagate across the grain boundaries. This is achieved by linearly coupling the micro-flexibility parameter C_Γ with the global phase-field d

$$C_\Gamma(d) = C_{\Gamma,0} + C_\Gamma^{\mathrm{d}}\, d\,. \tag{3.26}$$

Therein, $C_{\Gamma,0}$ is the initial micro-flexibility and C_Γ^{d} is a factor that controls the additional amount of micro-flexibility gained by complete material degradation. The linear coupling is here chosen for simplicity.

A noticeable simplification that has been taken in Paper C and Paper D is that grain boundaries act as plastic slip sinks. The models allow for slip transmission from the grains into the grain boundaries, but not the other way around. Slip is also not transmitted from grain to grain in these models. The presented modeling framework could be extended to account for these phenomena by adding interface elements along the grain boundaries. This could in particular be interesting when adopting a slip-system based gradient plasticity formulation like the one in Paper C together with micro-flexible boundary conditions as those presented in Paper D. For such a combination, it would be possible to express different geometric slip transmission criteria, see for example [20] for a discussion of different such criteria. However, modeling those effects adds a significant amount of complexity to the framework. Examples of particular problems with such an approach are the difficulty to parametrize such models, as well as the significant added computational cost.

Numerical example

Figure 3.6 shows an exemplary result from Paper D displaying the behavior of the ductile phase-field model with damage-dependent micro-flexible boundary conditions on a polycrystal. The left subfigure displays the degradation function at the end of the simulation, showing where cracks have developed. The right subfigure shows the accumulated plastic strain at the end of the simulation. The grain boundaries are color coded on a scale from white to black

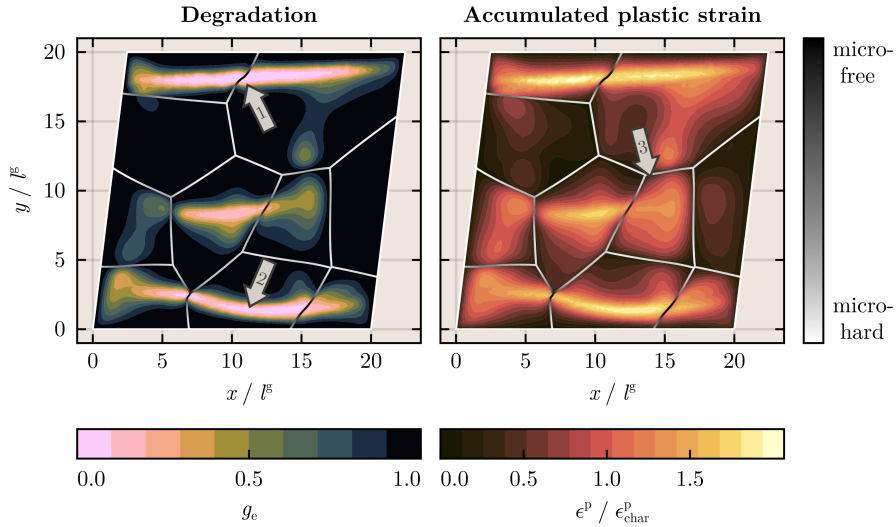

Figure 3.6: Example for ductile crack growth in a polycrystal with damage-dependent micro-flexible inner boundary conditions. The left side displays the degradation function at the end of the simulation, the right side shows the accumulated plastic strain distribution at the same point in time. Noticeable results are the local change of grain boundary behavior in the crack (arrow 1), the change of crack growth direction toward the stress concentration caused by the microstructure (arrow 2) and the remaining micro-hard grain boundary behavior in the less damaged region (arrow 3). The example is reprinted from Paper D, page 12.

indicating the local micro-hard to micro-free property. Originally, all grain boundaries are almost micro-hard ($C_{\Gamma,0} \to 0$). The inner grain boundaries can change their behavior locally during the simulation. The crack marked with arrow 1 develops first. It initiates in the right grain and then crosses the grain boundary to the left grain. A distinct s-shape of the broken grain boundary can be observed at the end of the simulation, showing the large deformations. Within the damage band the grain boundary behavior has locally changed to micro-free. This can also be recognized from the plastic strain distribution on the right. Further away from the heavily damaged zones, the grain boundary behavior is still mostly micro-hard. This can for example be

recognized well in the grain marked with arrow 3 on the right side of the figure. Arrow 2 marks the second crack that develops. It originates towards the right side of the middle grain, and then propagates to the left. The crack changes its crack growth direction during propagation and turns towards a stress concentration caused by the grain boundary intersection. The entire outer boundary is kept micro-hard throughout the simulation. None of the cracks propagates across these boundaries, displaying how micro-hard boundary conditions prevent crack growth across the corresponding boundaries.

CHAPTER 4

Concluding Remarks and Future Work

Nickel-based superalloys can experience intergranular fracture, transgranular fracture or a mixture of both fracture modes, depending on the specific loading conditions that they are exposed to. While transgranular fracture is typically the default fracture mode of these materials at room temperature, intergranular fracture occurs at high temperatures, paired with sustained tensile loading in oxygen-rich environments. Intergranular fracture is promoted by oxygen and is therefore referred to as environmentally assisted fracture. It causes a significant decrease of the mechanical properties and thereby reduces the life-time of components made from nickel-based superalloys. While the phenomenon has been known and experimentally investigated for many years, there has been limited work on numerical modeling of the interaction between the environmental oxygen and the mechanical behavior of polycrystalline nickel-based superalloys.

In this work, we present computational modeling frameworks for both fracture modes. The modeling framework for intergranular fracture predicts the interaction of oxygen, acting as an embrittling element, and its accelerating effect on the crack growth rate of polycrystals. The framework is based on chemo-mechanical phenomena which were inferred from a literature study of

various experimental results on intergranular fracture of nickel-based superalloys. The framework is thermodynamically consistent, and it has been shown in Paper A that it can qualitatively reproduce important experimental results, such as stress relaxation in oxygen-rich environments. In Paper B the framework is extended to allow for crack propagation and computation of crack growth rates. It has therein been demonstrated that the relations between the environmental oxygen content and the crack growth acceleration in the case of intergranular fracture can be predicted qualitatively correct for different dwell times during cyclic loading and different load levels. With these results, the first two research objectives formulated in Chapter 1 have been achieved.

In Paper C, a thermodynamic modeling framework for ductile phase-field fracture has been presented in a large deformation setting. The modeling framework is based on a gradient-enhanced crystal plasticity model, whereby it accurately represents the impact of crystal orientations and their effect on the anisotropic material behavior on the micro-scale, while the gradient-extension accounts for size effects. A micromorphic irreversibility strategy has been evaluated in Paper C, instead of employing, for example, a classical history variable approach. Therein, it has been shown that the micromorphic strategy yields reliable damage irreversibility in cyclic loading, if a sufficiently large penalty parameter is used. In Paper C, gradient-hardening along the slip directions is employed, while the formulation in Paper D uses isotropic gradient-hardening. These formulations result in similar hardening behavior for the studied cases, and the effect of micro-free versus micro-hard boundary conditions has been demonstrated for both formulations. However, the slip direction dependent gradient-hardening formulation requires the introduction of a global field for each slip system, whereby is causes a significantly higher computational cost compared to the isotropic gradient-extension. When extending the modeling framework to polycrystals, it has been shown that neither micro-free, nor micro-hard boundary conditions are suitable for accurately predicting fracture across grain boundaries. Micro-free boundary conditions do not correctly account for the grain size dependence (Hall-Petch effect), while micro-hard boundary conditions in combination with the employed degradation function prevent any damage development at the grain boundaries. Therefore, a damage-dependent micro-flexible boundary condition has been suggested in Paper D. This boundary condition reflects varying resistance of

the grain boundaries against slip transmission during the hardening stage, behaving similarly to a micro-hard boundary condition, and then recovers micro-free behavior during the softening stage, whereby it allows crack propagation across the grain boundaries. With these contributions, research objectives number 3 and 4 have been addressed in Papers C and D. Further, the capabilities of the modeling framework to account for material inhomogeneities and void coalescence, which are important phenomena in the formation of cracks, have been demonstrated in both these publications. While most of the presented simulation results are performed in a two-dimensional setting, crack fronts are in reality three-dimensional. The modeling framework is formulated in a dimension agnostic manner and in Paper C, as well as in Paper D, it has been demonstrated that it can be applied to three-dimensional problems. Finally, phase-field problems are known to be inherently non-convex and thereby difficult to solve in numerical frameworks. A common way to address the non-convexity is to employ a staggered solver and split the coupled problem into two convex problems, which is also the strategy that has been employed in this work. Paper D includes a detailed description of the features employed in the staggered solver in order to efficiently solve the phase-field problem.

Future work

Naturally, there are many possible research directions that have not been pursued in this thesis. Some of these possible directions for future work are discussed in this section.

Coupling of inter- and transgranular fracture models
Separate models have been developed for the inter- and transgranular fracture modes in this thesis. In order to simulate the full range of possible fracture behavior, it would be necessary to couple both models for predicting the mixed inter- and transgranular range. The interaction between the models would then function as follows: Undamaged grain boundaries have a higher strength than the bulk material. Thus the base fracture mechanism would be transgranular fracture. Upon oxygen exposure, the grain boundaries are weakened until they become weaker than the bulk material. If sufficiently much oxygen is supplied and it enters the structure sufficiently fast, fracture becomes purely intergranular. The mixed fracture region arises naturally when the (remain-

ing) strength of the grain boundaries and the bulk strength are similar. In that case microstructural details, such as grain geometries, slip system orientations etc. determine the exact crack path. A modeling framework that combines both presented models in particular needs to adequately address the combination of the cohesive zone model and the phase-field model. Paggi and Reinoso [52] have suggested a promising approach for this, where the critical opening gap of the cohesive zone model depends on the phase-field, which has subsequently been adopted for various problems, such as hydrogen-embrittlement in polycrystals [53], rock fracture [54] and fiber reinforced composites [55]. Further, transgranular fracture paths allow oxygen to flow into the grains. Modeling this would demand a generalization of the chemo-mechanical coupling in the grain boundaries to the bulk material, similar to what has been done for hydrogen embrittlement in Kristensen *et al.* [28].

Model parametrization and validation
A seemingly obvious extension of this work is the parametrization and subsequently the validation of the presented models against experimental data. However, both presented models include a significant number of parameters, many of which are complex to determine. Accurately parametrizing the crystal plasticity models requires in-situ testing on the micro-scale, for example by micro-beam bending or micro-pillar compression tests. Especially the grain boundary related parameters require similar tests, but in set-ups where the behavior of the grain boundary can be clearly distinguished from the grain behavior on either side. Those experiments also need to be conducted at high temperatures. This is an on-going research field on the experimental as well as on the numerical side. Accurate parametrization also requires the ability to conduct research in close collaboration between those fields.

Numerical stability
Fracture models are known to be difficult to solve in the softening regime. This is also true for the models presented in this thesis. In this work, monolithic (Paper A and Paper B) and staggered (Paper C and Paper D) Newton solvers have been employed. It is known that this class of solvers cannot handle snap-back behavior. Convergence problems before obtaining the final fracture state have been a common problem in the numerical examples. Possible remedies could be the use of arc-length solvers or a dynamic instead of quasi-static set-up. The chemo-mechanically coupled model additionally suffers from very steep concentration gradients close to the crack tip and also

from shock-wave like behavior in the oxygen field when the crack propagates. In the presented simulations, the problems related to the chemo-mechanical model have been addressed by a very fine grain boundary mesh and significant regularization incorporated in the moving boundary condition. Alternative solutions to these problems could be adaptive meshing in order to use a fine mesh resolution only close to crack tips and Upwind regularization schemes for the shock-wave behavior. Numerical difficulties are particularly problematic when widely varying parameter values are considered, for example in a parameter study or when adopting new specimen geometries / loading conditions.

Advanced grain boundary effects
In terms of the dislocation motion, the gradient-enhanced plasticity model in Paper C and Paper D takes the simplification that grain boundaries act as plastic slip sinks with varying degree of resistance against plastic slip transmission. This is a significant simplification compared to the dislocation motion observed at grain boundaries in reality, where dislocations can be transmitted into slip systems in a neighboring grain, be transmitted from a grain into the grain boundary or emitted from the grain boundary into a grain, be reflected at the grain boundary and also cause additional residual dislocations when interacting with the grain boundaries [20]. By extending the modeling framework by interface elements for the gradient fields and employing an approach similar to Paper C, where the plastic slip is described on a per slip system basis, it would be possible to capture some of these effects. The damage dependent micro-flexible boundary condition could then also be used in order to express geometric slip transmission criteria. Such detailed grain boundary models however come at the cost of an increased number of parameters, which are challenging to determine, as outlined above, and a considerably increased computational cost.

Fatigue
Intergranular fracture of nickel-based superalloys is often considered to be a fatigue phenomenon, since the required sustained tensile loading often occurs as a part of the loading cycle. The impact of a sustained tensile loading phase during cyclic loading has for example been studied in Paper B. Classical metal fatigue on the other hand has not been considered in this thesis. In the future, it would be an interesting, but complex addition to the transgranular fracture model. Fatigue modeling coupled to phase-field fracture modeling is a relatively new research field. On top of the added model complexity, fatigue

simulations require resolving thousands to millions of loading cycles, making it a computationally extremely expensive problem, often requiring acceleration techniques such as cycle jumping.

References

[1] J. Hall, "Safety Recommendation, A-00-121 through -124, GE CF6-80C2B2 engine failure," *NTSB Safety Recommendation*, 2000.

[2] Australian Transport Safety Bureau, "In-flight uncontained engine failure and air turn-back, Boeing 767-219ER, ZK-NBC 8," *Aviation Safety Investigation Report*, no. 200205780, 2002.

[3] M. V. Rosenker, "A-06-60 to -64, Report on General Electric CF6-80A engine failure from June 2, 2006," *NTSB Safety Recommendation*, 2006.

[4] Jean-Pierre Scarfo, "NTSB Powerplant Group Chairman's factual report, General Electric GE90-85BG11 turbofan engine failure," *NTSB Factual Report*, 2016.

[5] B. G. Gieseke, "METALLURGICAL EVALUATION OF CF6-80A HPT STAGE 1 DISK / SHAFT DISK SEPARATION EVENT AT LAX ON JUNE 2 , 2006," *GE Aviation, MPED-Metallurgical Investigations*, 2006.

[6] D. Kramer, "Report No. 15-131, General Electric GE90-85BG11 turbofan engine failure," *NTSB Materials Laboratory factual report*, no. Report No. 15-131, 2016.

[7] C. T. Liu and C. L. White, "Dynamic embrittlement of boron-doped Ni3Al alloys at 600°C," *Acta Metallurgica*, vol. 35, no. 3, pp. 643–649, 1987, ISSN: 00016160.

[8] E. Andrieu, R. Molins, H. Ghonem, and A. Pineau, "Intergranular crack tip oxidation mechanism in a nickel-based superalloy," vol. 154, pp. 21–28, 1992, ISSN: 09215093.

[9] J. A. Pfaendtner and J. J. McMahon, "Oxygen-induced intergranular cracking of a Ni-base alloy at elevated temperatures - An example of dynamic embrittlement," *Acta Materialia*, vol. 49, no. 16, pp. 3369–3377, 2001, ISSN: 13596454.

[10] A. Pineau and S. D. Antolovich, "High temperature fatigue of nickel-base superalloys - A review with special emphasis on deformation modes and oxidation," *Engineering Failure Analysis*, vol. 16, no. 8, pp. 2668–2697, 2009, ISSN: 13506307.

[11] R. Molins, G. Hochstetter, J. C. Chassaigne, and E. Andrieu, "Oxidation effects on the fatigue crack growth behaviour of alloy 718 at high temperature," *Acta Materialia*, vol. 45, no. 2, pp. 663–674, 1997, ISSN: 13596454.

[12] H. Ghonem and D. Zheng, "Depth of intergranular oxygen diffusion during environment-dependent fatigue crack growth in alloy 718," *Materials Science and Engineering A*, vol. 150, no. 2, pp. 151–160, 1992, ISSN: 09215093.

[13] J. J. Moverare and D. Gustafsson, "Hold-time effect on the thermo-mechanical fatigue crack growth behaviour of Inconel 718," *Materials Science and Engineering A*, vol. 528, no. 29-30, pp. 8660–8670, 2011, ISSN: 09215093.

[14] H.-J. Christ, K. Wackermann, and U. Krupp, "Materials at High Temperatures Effect of dynamic embrittlement on high temperature fatigue crack propagation in IN718-experimental characterisation and mechanism-based modelling Effect of dynamic embrittlement on high temperature fatigue crack propagation," 2016, ISSN: 1878-6413.

[15] L. Viskari, M. Hörnqvist, K. L. Moore, Y. Cao, and K. Stiller, "Intergranular crack tip oxidation in a Ni-base superalloy," *Acta Materialia*, vol. 61, no. 10, pp. 3630–3639, 2013, ISSN: 13596454.

[16] M. Hörnqvist, L. Viskari, K. L. Moore, and K. Stiller, "High-temperature crack growth in a Ni-base superalloy during sustained load," *Materials Science and Engineering A*, vol. 609, pp. 131–140, 2014, ISSN: 09215093.

[17] L. Viskari, Y. Cao, M. Norell, G. Sjöberg, and K. Stiller, "Grain boundary microstructure and fatigue crack growth in Allvac 718Plus superalloy," *Materials Science and Engineering A*, vol. 528, no. 6, pp. 2570–2580, 2011, ISSN: 09215093.

[18] A. Pineau, A. A. Benzerga, and T. Pardoen, "Failure of metals I: Brittle and ductile fracture," *Acta Materialia*, vol. 107, pp. 424–483, 2016, ISSN: 13596454.

[19] A. Rovinelli, M. D. Sangid, H. Proudhon, and W. Ludwig, "Using machine learning and a data-driven approach to identify the small fatigue crack driving force in polycrystalline materials," *npj Computational Materials*, vol. 4, no. 1, pp. 1–10, 2018, ISSN: 20573960.

[20] E. Bayerschen, a. T. McBride, B. D. Reddy, and T. Böhlke, "Review on slip transmission criteria in experiments and crystal plasticity models," *Journal of Materials Science*, 2015, ISSN: 0022-2461.

[21] O. Aslan, N. M. Cordero, A. Gaubert, and S. Forest, "Micromorphic approach to single crystal plasticity and damage," *International Journal of Engineering Science*, vol. 49, no. 12, pp. 1311–1325, 2011, ISSN: 00207225.

[22] C. Miehe, F. Welschinger, and M. Hofacker, "Thermodynamically consistent phase-field models of fracture: Variational principles and multi-field FE implementations," *International Journal for Numerical Methods in Engineering*, vol. 83, pp. 1273–1311, 2010.

[23] C. Miehe, M. Hofacker, and F. Welschinger, "A phase field model for rate-independent crack propagation: Robust algorithmic implementation based on operator splits," *Computer Methods in Applied Mechanics and Engineering*, vol. 199, no. 45-48, pp. 2765–2778, 2010, ISSN: 00457825.

[24] R. Alessi, M. Ambati, T. Gerasimov, S. Vidoli, and L. De Lorenzis, "Comparison of phase-field models of fracture coupled with plasticity," in *Computational Methods in Applied Sciences*, vol. 46, 2018, pp. 1–21, ISBN: 9783319608853.

[25] R. de Borst and C. V. Verhoosel, "Gradient damage vs phase-field approaches for fracture: Similarities and differences," *Computer Methods in Applied Mechanics and Engineering*, vol. 312, pp. 78–94, 2016, ISSN: 00457825.

[26] X. P. Xu and A. Needleman, "Void nucleation by inclusion debonding in a crystal matrix," *Modelling and Simulation in Materials Science and Engineering*, vol. 1, no. 2, pp. 111–132, 1993, ISSN: 1361651X.

[27] M. Kolluri, J. P. Hoefnagels, J. A. Van Dommelen, and M. G. Geers, "Irreversible mixed mode interface delamination using a combined damage-plasticity cohesive zone enabling unloading," *International Journal of Fracture*, vol. 185, no. 1-2, pp. 77–95, 2014, ISSN: 03769429.

[28] P. K. Kristensen, C. F. Niordson, and E. Martínez-Pañeda, "A phase field model for elastic-gradient-plastic solids undergoing hydrogen embrittlement," *Journal of the Mechanics and Physics of Solids*, vol. 143, 2020, ISSN: 00225096.

[29] P. Sofronis and R. M. McMeeking, "Numerical analysis of hydrogen transport near a blunting crack tip," *Journal of the Mechanics and Physics of Solids*, vol. 37, no. 3, pp. 317–350, 1989, ISSN: 00225096.

[30] S. Serebrinsky, E. A. Carter, and M. Ortiz, "A quantum-mechanically informed continuum model of hydrogen embrittlement," *Journal of the Mechanics and Physics of Solids*, vol. 52, no. 10, pp. 2403–2430, 2004, ISSN: 00225096.

[31] S. del Busto, C. Betegón, and E. Martínez-Pañeda, "A cohesive zone framework for environmentally assisted fatigue," *Engineering Fracture Mechanics*, vol. 185, pp. 210–226, 2017, ISSN: 00137944.

[32] L. G. Zhao, "Modeling of oxygen diffusion along grain boundaries in a nickel-based superalloy," *Journal of Engineering Materials and Technology, Transactions of the ASME*, vol. 133, no. 3, pp. 24–26, 2011, ISSN: 00944289.

[33] A. Karabela, L. G. Zhao, B. Lin, J. Tong, and M. C. Hardy, "Oxygen diffusion and crack growth for a nickel-based superalloy under fatigue-oxidation conditions," *Materials Science and Engineering A*, vol. 567, pp. 46–57, 2013, ISSN: 09215093.

[34] A. Golahmar, P. K. Kristensen, C. F. Niordson, and E. Martínez-Pañeda, "A phase field model for hydrogen-assisted fatigue," *International Journal of Fatigue*, vol. 154, no. August 2021, 2022, ISSN: 01421123.

[35] C. Kuhn, T. Noll, and R. Müller, "On phase field modeling of ductile fracture," *GAMM Mitteilungen*, vol. 39, no. 1, pp. 35–54, 2016, ISSN: 15222608.

[36] C. Miehe, S. Teichtmeister, and F. Aldakheel, "Phase-field modelling of ductile fracture: A variational gradient-extended plasticity-damage theory and its micromorphic regularization," *Philosophical Transactions of the Royal Society A: Mathematical, Physical and Engineering Sciences*, vol. 374, no. 2066, 2016, ISSN: 1364503X.

[37] M. J. Borden, T. J. Hughes, C. M. Landis, A. Anvari, and I. J. Lee, "A phase-field formulation for fracture in ductile materials: Finite deformation balance law derivation, plastic degradation, and stress triaxiality effects," *Computer Methods in Applied Mechanics and Engineering*, vol. 312, pp. 130–166, 2016, ISSN: 00457825.

[38] T. Maloth and S. Ghosh, "Coupled Crystal Plasticity Phase-Field Model for Ductile Fracture in Polycrystalline Microstructures," *International Journal for Multiscale Computational Engineering*, vol. 21, no. 2, pp. 1–19, 2023, ISSN: 15431649.

[39] M. Ambati, T. Gerasimov, and L. De Lorenzis, "Phase-field modeling of ductile fracture," *Computational Mechanics*, vol. 55, no. 5, pp. 1017–1040, 2015, ISSN: 01787675.

[40] B. Bourdin, G. A. Francfort, and J. J. Marigo, "The variational approach to fracture," *Journal of Elasticity*, vol. 91, no. 1-3, pp. 5–148, 2008.

[41] M. F. Wheeler, T. Wick, and W. Wollner, "An augmented-Lagrangian method for the phase-field approach for pressurized fractures," *Computer Methods in Applied Mechanics and Engineering*, vol. 271, pp. 69–85, 2014, ISSN: 00457825.

[42] T. Gerasimov and L. De Lorenzis, "On penalization in variational phase-field models of brittle fracture," *Computer Methods in Applied Mechanics and Engineering*, vol. 354, pp. 990–1026, 2019, ISSN: 00457825.

[43] L. De Lorenzis and T. Gerasimov, "Numerical Implementation of Phase-Field Models of Brittle Fracture," in *Modeling in Engineering using Innovative Numerical Methods for Solids and Fluids*, L. De Lorenzis and A. Düster, Eds., Udine: Springer, 2020, ch. Numerical, pp. 75–101.

[44] S. Forest, "Micromorphic Approach for Gradient Elasticity, Viscoplasticity, and Damage," *Journal of Engineering Mechanics*, vol. 135, no. 3, pp. 117–131, 2009, ISSN: 0733-9399.

[45] C. Miehe, F. Aldakheel, and S. Teichtmeister, "Phase-field modeling of ductile fracture at finite strains: A robust variational-based numerical implementation of a gradient-extended theory by micromorphic regularization," *International Journal for Numerical Methods in Engineering*, vol. 111, no. 9, pp. 816–863, 2017.

[46] R. Bharali, F. Larsson, and R. Jänicke, "A micromorphic phase-field model for brittle and quasi-brittle fracture," *Computational Mechanics*, 2023, ISSN: 14320924.

[47] L. De Lorenzis, A. McBride, and B. D. Reddy, "Phase-field modelling of fracture in single crystal plasticity," *GAMM Mitteilungen*, vol. 39, no. 1, pp. 7–34, 2016, ISSN: 09367195.

[48] C. Miehe, F. Aldakheel, and A. Raina, "Phase field modeling of ductile fracture at finite strains: A variational gradient-extended plasticity-damage theory," *International Journal of Plasticity*, vol. 84, pp. 1–32, 2016, ISSN: 07496419.

[49] K. Carlsson, K. Runesson, F. Larsson, and M. Ekh, "A comparison of the primal and semi-dual variational formats of gradient-extended crystal inelasticity," *Computational Mechanics*, vol. 60, no. 4, pp. 531–548, 2017, ISSN: 01787675.

[50] M. Ekh, M. Grymer, K. Runesson, and T. Svedberg, "Gradient crystal plasticity as part of the computational modelling of polycrystals," *International Journal for Numerical Methods in Engineering*, vol. 72, no. 2, pp. 197–220, 2007.

[51] M. Ekh, S. Bargmann, and M. Grymer, "Influence of grain boundary conditions on modeling of size-dependence in polycrystals," *Acta Mechanica*, vol. 218, no. 1-2, pp. 103–113, 2011, ISSN: 00015970.

[52] M. Paggi and J. Reinoso, "Revisiting the problem of a crack impinging on an interface: A modeling framework for the interaction between the phase field approach for brittle fracture and the interface cohesive zone model," *Computer Methods in Applied Mechanics and Engineering*, vol. 321, pp. 145–172, 2017, ISSN: 00457825.

[53] A. Valverde-González, E. Martínez-Pañeda, A. Quintanas-Corominas, J. Reinoso, and M. Paggi, "Computational modelling of hydrogen assisted fracture in polycrystalline materials," *International Journal of Hydrogen Energy*, vol. 47, no. 75, pp. 32 235–32 251, 2022.

[54] J. Reinoso, P. Durand, P. R. Budarapu, and M. Paggi, "Crack patterns in heterogenous rocks using a combined phase field-cohesive interface modeling approach: A numerical study," *Energies*, vol. 12, no. 6, 2019, ISSN: 19961073.

[55] T. Guillén-Hernández, I. G. García, J. Reinoso, and M. Paggi, "A micromechanical analysis of inter-fiber failure in long reinforced composites based on the phase field approach of fracture combined with the cohesive zone model," *International Journal of Fracture*, vol. 220, no. 2, pp. 181–203, 2019, ISSN: 15732673.